Article

Bubble-Mediated Ultrasensitive Multiplex Detection of Metal Ions in Three-Dimensional DNA Nanostructure-Encoded Microchannels

Xiangmeng Qu, Fan Yang, Hong Chen, Jiang Li, Hongbo Zhang, Guo-Jun Zhang, Li Li, Lihua Wang, Shiping Song, Yang Tian, and Hao Pei

ACS Appl. Mater. Interfaces, **Just Accepted Manuscript** • Publication Date (Web): 21 Apr 2017

Bubble-Mediated Ultrasensitive Multiplex Detection of Metal Ions in Three-Dimensional DNA Nanostructure-Encoded Microchannels

Xiangmeng Qu,[1,2‡] Fan Yang,[3‡] Hong Chen,[1] Jiang Li,[4] Hongbo Zhang,[5] Guojun Zhang,[3] Li Li,[2] Lihua Wang,[4] Shiping Song,[4] Yang Tian,[2] Hao Pei[2]**

[1]Pen-Tung Sah Institute of Micro-Nano Science and Technology of Xiamen University, Xiamen University, Xiamen, 361005, P. R. China
[2]Shanghai Key Laboratory of Green Chemistry and Chemical Processes, School of Chemistry and Molecular Engineering, East China Normal University, 500 Dongchuan Road, Shanghai, 200241, P. R. China
[3]School of Laboratory Medicine, Hubei University of Chinese Medicine, Wuhan, 430065, P. R. China
[4]Division of Physical Biology & Bioimaging Center, Shanghai Synchrotron Radiation Facility, Shanghai Institute of Applied Physics, Chinese Academy of Sciences, Shanghai, 201800, P. R. China
[5]Department of Pharmaceutical Science, Åbo Akademic University, FI-20520, Turku, Finland

Keywords: DNA nanostructures, Microchannel, Microarray, Multiplex detection, Metal ions

ABSTRACT: The development of rapid and sensitive point-of-test devices for the on-site monitoring of heavy-metal contamination has great scientific and technological importance. However, developing fast, inexpensive, and sensitive microarray sensors to achieve such goal remains challenging. In this work, we present a DNA nanostructured microarray (DNM) with tubular three-dimensional (3D) sensing surface and ordered nanotopography. This microarray enables enhanced molecular interaction toward the rapid and sensitive multiplex detection of heavy-metal ions. In our design, the use of DNA tetrahedral-structured probes (TSPs) engineers the sensing interface with spatially resolved and density-tunable sensing spots that improve the microconfined molecular recognition. A bubble-mediated shuttle reaction was used inside the DNM functionalized microchannel to improve the target-capturing efficiency. By using this novel DNM biosensor, the sensitive and selective detection of multiple heavy-metal ions (i.e., Hg^{2+}, Ag^{+}, and Pb^{2+}) were achieved within 5 min, the detection limit was down to 10 nM, 10 nM and 20 nM for Hg^{2+}, Ag^{+} and Pb^{2+}, respectively. The feasibility of our DNM sensor was further demonstrated by probing heavy-metal ions in real water samples with a direct optical readout. Beyond metal ions, this unique DNM sensor can easily be extended to in vitro bioassays and clinical diagnostics.

INTRODUCTION

The development of rapid and sensitive sensors for the on-site monitoring of environmental toxins including heavy-metal contamination is critically important to human health and ecological system.[1-8] Such contamination usually involves multiple toxic

ingredients requiring a multiplex detection strategy for the simultaneous readout of varied targets of interest.[9-12] Traditional microarray platform has shown its powerful high-throughput assay ability mainly due to the developed construction of multiplex sensing interfaces and fluorescence imaging.[13-17] However, rationally building a user-friendly microarray sensor with attractive speed and sensitivity remains a hurdle.[18-22]

Particularly, engineering a heterogeneous sensing interface that promotes the kinetics and thermodynamics of probe–target interactions urgent need to engineer.[23-27] Notably, sensor performance was limited by the affinity between targets and surface-tethered probes[28-29] and by interfacial properties such as the orientation, ordering and density of probes, as well as the diffusion rate of the target of interest.[23, 30-32] For instance, mass transport is dominated by linear diffusion at macroscopic interfaces but by isotropical radial diffusion at micro- or nanoscopic interfaces.[23-24] Therefore, with reduced sensor size to nanoscale, mass transport rate and detection sensitivity can be dramatically increased.[33-34] However, a nanosensor with extremely small effective surface area can support only a limited amount of probes, which restricts the probability of collision and binding between surface-tethered probes and freely diffused target analytes.[30] Intermolecular colliding event or recognition occurs within the nanometer range (often within 10 nm), and molecules can typically diffuse 10–100 μm in solution.[35] Thus, to address this "size dilemma," a trans-scale design of sensor that integrates nanoscopic features onto macroscopic surfaces is a prerequisite. In this case, probe–target recognition can be greatly improved once the dynamic targets are closely confined to the static surface-tethered nanoprobes arranged in macroscale. Considering the radial-diffusion

feature of analytes at micro- or nanoscale interface, we assume that rolling up a traditional two-dimensional (2D) planar sensing surface into a 3D tubular inner sensing surface is expected to improve the sensor performance even further.[36-38] Given that a higher collision rate between probes and target analytes occurs in the microconfined settings, the tailor engineering of an ordered and finely tunable nanostructured molecular recognition interface is highly desirable to better harness such an advantage.

In recent years, self-assembled DNA nanostructures have demonstrated great potential in the development of biosensors and devices owing to their unparalleled capabilities in molecular recognition and programmable sensing interface engineering.[39-43] In the present work, we exquisitely designed a spatially resolved 3D tubular DNA nanostructured microarray (DNM) functionalized microchannel for the rapid and sensitive multiplex detection of heavy-metal ions. To construct the DNM, target-specific DNA tetrahedral structured probes (TSPs) were rapidly self-assembled and incorporated into a droplet array[44-47] and then moved to the designated locations for immobilization and sensing-interface engineering.[48] The spatially resolved and density-tunable DNM were evenly spaced along the microchannel with highly ordered probe orientations and circular arrangement. This setup endowed the microconfined microarray sensor with improved sensitivity and selectivity. To enhance probe–target interactions, a low-cost bubble-based shuttle reaction strategy was used inside microchannels by using air bubbles to separate multiple reagent plugs. This bubble-mediated strategy avoided the need to design and fabricate complex microchannel, as well as the requirement of extensive user intervention, rendering the strategy attractive for the development of point-of-care test (POCT)

devices.[49] Finally, we demonstrate the practical utilization of this DNM sensor for the sensitive and selective multiplex detection of heavy-metal ions in river water samples.

EXPERIMENTAL SECTION

Chemicals and Materials. Tris(hydroxymethyle)aminomethane, Pb(II) nitrate, silver nitrate and mercury(II) perchloride monohydrate were purchased from Sigma–Aldrich. $Na_2HPO_4 \cdot 12H_2O$, $NaH_2PO_4 \cdot 2H_2O$, NaCl, and $MgCl_2$, were purchased from West Long Chemical Co., Ltd. (Guangzhou, China). Then, 100 mL of 10 mM phosphate buffer (pH 7.4) solution was prepared by mixing 81 mL of 10 mM aqueous Na_2HPO_4 with 19 mL of 10 mM aqueous NaH_2PO_4. All oligonucleotides were synthesized and purified by Sangon Biotech Shanghai Co., Ltd. (Shanghai, China), and the sequences are shown as below:

Table 1. Sequences of DNA Tetrahedral-Structured (TSP) Probes

Oligo	Sequence (5′-3′)
TSP-A	Probe-ACATTCCTAAGTCTGAAACATTACAGCTTGCTACACGAGAAGAGCCGCCATAGTA
TSP-B	NH2-C6-TATCACCAGGCAGTTGACAGTGTAGCAAGCTGTAATAGATGCGAGGGTCCAATAC
TSP –C	NH2-C6-TCAACTGCCTGGTGATAAAACGACACTACGTGGGAATCTACTATGGCGGCTCTTC
TSP –D	NH2-C6-TTCAGACTTAGGAATGTGCTTCCCACGTAGTGTCGTTTGTATTGGACCCTCGCAT

Table 2. Sequences of DNA Tetrahedral-Structured (TSP) Probes and reporter DNA

Description	Oligo DNA	Sequence (5′-3′)
Mercury ion assay	TSP-A1 (mercury ion specific sequence)	TTCGTTCCTGTTTGCGAAAAAAAAAAAACATTCCTAAGTCTGAAACAT TACAGCTTGCTACACGAGAAGAGCCGCCATAGTA
	Reporter sequence	CGCATTCAGGTTCGTA-Cy3
Silver ion assay	TSP-A2 (silver ion specific sequence)	CACACACACACACACACACACAAAAAAAAAAAACATTCCTAAGTCTGA AACATTACAGCTTGCTACACGAGAAGAGCCGCCATAGTA
	Reporter sequence	CTCTCTCTCTCTCTCTCTCTC-Cy3
Pb ion assay	TSP-A3 (Pb ion specific sequence)	CATCTCTTCTCCGAGCCGGTCGAAATAGTGAGTCAGACATATTTTTTTT TTACATTCCTAAGTCTGAAACATTACAGCTTGCTACACGAGAAGAGCC GCCATAGTA

Substrate strand	TATGTCTGACTCACTTArAGGAAGAGATGTATGTCTGACTCACTTAGGA
Reporter sequence	AGAGATG-Cy3

Synthesis of DNA Tetrahedral Structured Probes (TSPs). In a typical procedure, the four oligonucleotides (TSP-A, TSP-B, TSP-C, and TSP-D) were mixed stoichiometrically and dissolved in TM buffer (20 mM Tris, 50 mM $MgCl_2$, pH 8.0), yielding a final concentration of 50 μM. The sequences specific to target ions (Hg^{2+} or Ag^{+}) were used as the extension of TSP-A at one vertex of DNA tetrahedron. For the Pb-ion analysis, the Pb-ion specific sequence and its substrate strand were used to form hybridization duplex and used as the extension at one vertex of DNA tetrahedron. The resulting solution was heated to 95 °C for 2 min and cooled to 4 °C in 30 s.

Bubble-Mediated Shuttle Reaction Process. The DNM functionalized capillary was connected to the as-prepared sample plugs array via the inlet and subsequently connected to a syringe pump (LongerPump, LSP02-1B) via the outlet. A flow rate of 5 μL/min was used to drive the sample plug array from the inlet. The sample plug array contained an aqueous solution plug of metal ions (10 μL in various concentrations) and Cy3-labeled reporter (5 μL, 1.5 μM), an air bubble plug, and a solution plug of washing buffer (20 mM Tris-HCl buffer). Here, pH 7.0 was used as the optimum reaction condition to avoid the hydroxyl precipitation reaction of heavy-metal ions under alkaline condition, and unfavorable structural changes of DNA under acidic condition.[50] The sample plugs array moved successively through the DNM sensing interface. The syringe pump was paused when the sample plugs array approached the outlet of the capillary. The sample plugs array then flowed backwards through the DNM sensing interface at a flow rate of 5 μL/min. The

process can be repeat multiple times until the DNM functionalized capillary was ready for fluorescence assay. The recognition capability of the TSP-based sensor was tested against the ssDNA probe-based sensor. The selectivity of the TSP-based sensor was tested in the presence of the competing metal ions, including Mg^{2+}, Ag^{+}, Ca^{2+}, Hg^{2+}, Cu^{2+}, Fe^{3+}, Ni^{2+} and Co^{2+}. The concentration of interfering ions was all set to 2 μM.

Fluorescence Microscopic Imaging. A confocal laser fluorescence microscope (Typhoon 9210) was utilized to evaluate the efficiency of DNM sensor for metal-ion assay. Fluorescence signal was recorded at an excitation wavelength of 532 nm with a resolution of 10 μm. Fluorescence intensity at an emission wavelength of 580 nm was used for quantitative analysis, and fluorescent images were analyzed using ImageQuant software.

RESULTS AND DISCUSSION

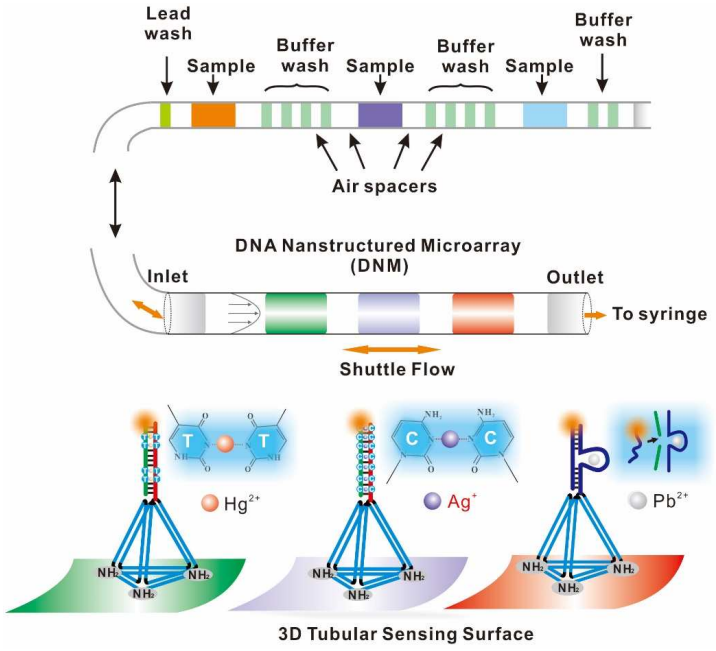

Scheme 1. Construction of 3D tubular DNM sensor inside microchannels for the detection

of Hg^{2+}, Ag^{+}, and Pb^{2+} based on bubble-mediated shuttle reaction.

By adapting a series of metal-ion specific sequences to DNA tetrahedron (Scheme 1), we constructed 3D tubular DNM sensor inside microchannels for the detection of Hg^{2+}, Ag^{+}, and Pb^{2+}.[51] DNA TSPs were assembled with four different DNA sequences following previous reports.[52-55] Amine groups at three vertices of TSPs were used to immobilize DNM on an aldehyde-functionalized microchannel. Specifically, for Hg^{2+} detection (Scheme 1 and Figure 1A), we used the Hg-ion specific oligonucleotide (TSP-A1) and a Cy3-labeled reporter that is rich in thymines and readily forms T-Hg^{2+}-T configuration in the presence of target Hg ions.[56-60] Interestingly, the TSP-based sensor exhibited approximately two times improvement in sensitivity compared with ssDNA probe-based sensor (Figure 1B). This improvement was ascribed to the highly ordered upright orientation of TSPs at the sensing interface, thereby accommodating the pendant probe DNA with a solution-phase-like environment inside microchannel; whereas ssDNA probes inclined to lie flat at the sensing interface, resulting in much lower capture efficiency.[30] DNM sensor performance was then evaluated at varying target concentrations. As shown in Figure 1C, fluorescence intensity nonlinearly increased with increased Hg^{2+} concentration, and exhibited good exponential response from 10 nM to 200 nM, with a detection limit of 10 nM. The binding constant (K_a) was determined from fluorescence titration plot as 2.36×10^{7} M^{-1} for Hg^{2+}. To further evaluate the selectivity of the DNM sensor, a variety of metal ions including Ag^{+}, Cu^{2+}, Pb^{2+}, Ca^{2+}, Mg^{2+}, Fe^{3+}, Ni^{2+}, and Co^{2+} were added into the system, and fluorescence signals were collected. As shown in Figure 1D, this system exhibited excellent selectivity toward Hg^{2+} by a factor of 10-fold compared with other

metal ions. Interestingly, the DNM sensor can be easily regenerated by adding cysteine which can selectively coordinate with Hg^{2+} and extract it from the T-Hg^{2+}-T complex due to stronger interactions.[61]

To establish a rapid assay for metal-ion detection, we applied bubble-mediated shuttle reaction inside microchannels (Scheme 1). As the test bed, we used the DNM sensor for Hg-ion analysis (Figure 1E). The discrete sample plugs consisted of three plugs, including an aqueous sample solution (Hg^{2+} ion and Cy3-labeled reporter), an air bubble, and a washing buffer solution. These plugs were shuttled back and forth along the microchannel using a syringe pump, sweeping over DNM while recirculation mixing occurred inside the plugs.[62] At a fixed flow rate of 5 μL/min, the number of recirculation of sample plugs passing through the sensor surface defined the efficiency of the reaction. Fluorescence intensity exhibited a nonlinear increase with shuttle hybridization time. Importantly, we found that shuttle hybridization exceeding 5 min led to a saturated signal at a flow rate of 5 μL/min, and the utilization of the shuttle reaction inside microchannel considerably reduced the reaction time from 30 min to 5 min.[63] By contrast, at least 12 hours passed before completion of hybridization in the case of conventional 2D microarray.

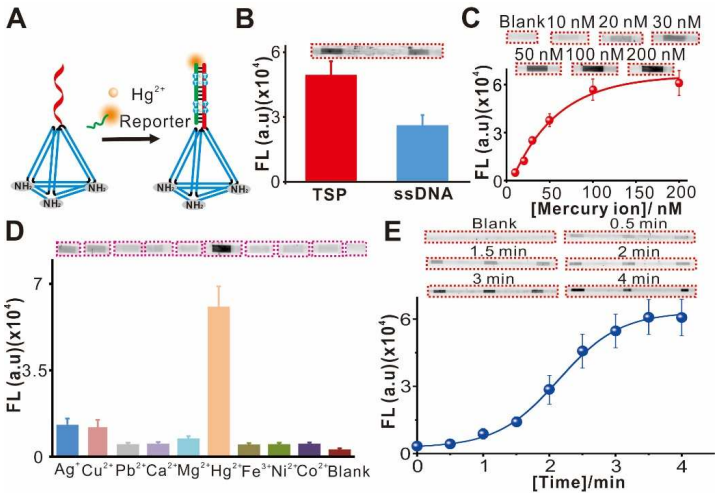

Figure 1. 3D tubular DNM sensor for Hg-ion assay. (A) The presence of Hg ions is transduced to fluorescence signals through the formation of T-Hg^{2+}-T configuration. (B) Comparison of TSP- and ssDNA probe-based sensor performance (with 100 nM Hg^{2+}). The inset displays the corresponding fluorescent images. (C) Fluorescence intensities and corresponding fluorescent images (shown as inset) of DNM sensing spots in the presence of Hg^{2+} at 10, 20, 30, 50, 100, or 200 nM. (D) Selectivity of DNM-based Hg^{2+} sensor over different metal ions. (E) Fluorescence intensity vs. shuttle hybridization time (with 200 nM Hg^{2+}). The inset displays the fluorescent images of three different DNM sensing spots inside microchannels at corresponding hybridization times.

For Ag^{+} detection, we designed a cytosine-rich silver-ion specific oligonucleotide[16] (TSP-A2) at one vertex of TSP and a Cy3-lableled reporter rich in cytosine based on the C-Ag^{+}-C interaction (Scheme 1 and Figure 2A). In the same pattern, for Pb^{2+} detection, we used a Pb-ion specific oligonucleotide (TSP-A3), its substrate strand, and a Cy3-labled reporter. The substrate strand was cleaved in the presence of Pb^{2+} and dissociated from the duplex, followed by substitution with the Cy3-labled reporter, resulting in duplex

hybridization with the remaining Pb-ion specific oligonucleotide (Scheme 1 and Figure 2D).[64] We then interrogated their detection capability for Ag^+ and Pb^{2+}, respectively. Fluorescence intensity monotonously increased with increased Ag^+ concentration from 10 nM to 400 nM, where the binding constant for sensing Ag^+ was determined as 2.16×10^7 M^{-1} (Figure 2B). Controlled experiments revealed that interfering ions led to negligible responses, suggesting the remarkable selectivity of the DNM sensor (Figure 2C). Similarly, the Pb^{2+}-responsive TSP-based sensor was applied for Pb-ion assay and showed high discrimination against eight different metal ions (Figures 2E and 2F). And the binding constant was determined as 5.2×10^6 M^{-1} for Pb^{2+}. Importantly, this DNM sensor exhibited excellent sensitivity, with a remarkable detection limit of 10 nM and 20 nM toward Ag^+ and Pb^{2+}, both of which were significantly lower than the recommended standard of the US EPA for drinking water (Ag^+, 464 nM; Pb^{2+}, 72 nM).[65] Taken together, these results indicated that the DNM sensor allowed for the highly sensitive and selective detection of various heavy-metal ions.

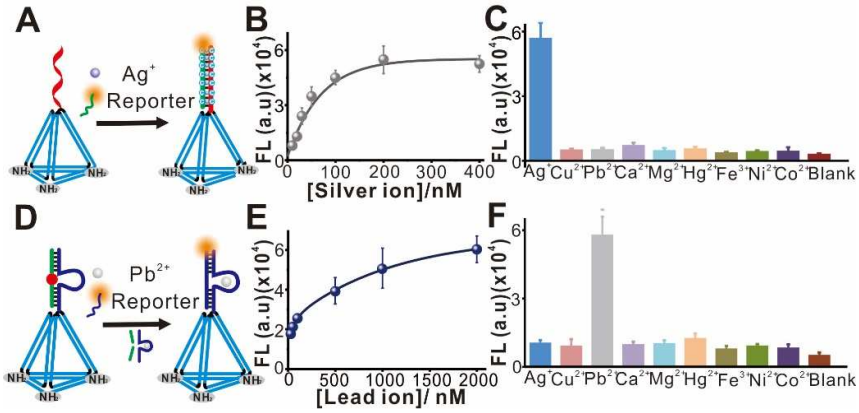

Figure 2. 3D tubular DNM sensor for silver and Pb-ion assay. (A) The presence of silver ions was transduced to fluorescence signals through the formation of C-Ag^+-C

configuration. (B) Fluorescent spectra of the DNM-based Ag^+ sensor upon addition of Ag^+ (10, 20, 30, 50, 100, 200, or 400 nM). (C) Selectivity of the DNM-based Ag^+ sensor over different metal ions. (D) Detection scheme for Pb ions. (E) Fluorescence intensities in the presence of Pb^{2+} (20, 50, 100, 500, 1000, or 2000 nM). (F) Selectivity of the DNM-based Pb^{2+} sensor over different metal ions.

To optimize the performance of the DNM sensor for heavy-metal ion detection, we also investigated one of the most critical parameters, i.e., the concentration of Cy3-labeled reporter. Taking the silver-ion assay as an example, we tested a series of concentrations of Cy3-labeled reporter incubated with 10 μM DNA TSP and 200 nM Ag ions (Figure S1 in Supporting Information). We found that the fluorescence signal gradually increased with increased Cy3-labeled reporter concentration and stabilized at 5 μM. Thus, 5 μM was deemed as the optimum concentration of Cy3-labled reporter for further experiments.

Having established the sensing capability of the DNM sensor, we further carried out theoretical studies on the DNA hybridization of target analyte solution with sensing interface inside microchannels. The paradigmatic model system is illustrated in Figure 3A. The target analyte solution flowed through a microchannel of inner diameter *D* and whose wall contained a tubular 3D sensing surface of length *L* in the flow direction. The key parameters for simulation was established based on our sensing system, in which the surface density of the tubular 3D sensing surface was 1×10^{-7} mol/m^2 and both length *L* and inner diameter *D* were 200 μm. The target analyte solution was pressure driven into the microchannel. The concentration and diffusion coefficient of the target analyte solution were 1 μM and 10^{-11} m^2/s, respectively. We initially examined the effect of purely diffusive

flux with a setup velocity υ of 0 mm/s under a series of reaction times, including 10, 30, 70, 160, 380, and 900 s, in which 900 s was the time for all probes on the tubular sensing surface to complete the reaction. As shown in Figure 3B, a depleted zone was formed as soon as target analytes were collected by sensing probes on the surface (10 s). The target analytes were then continuously diffused into the depleted zone under a concentration gradient until the sensing probes were completely consumed (900 s). In this scenario, the reaction rate of target analytes and sensing probes was less than the diffusion rate of target analytes, so the reaction time was determined by the diffusion rate of target analytes.[23] According to the general formula $t = l^2/d$ (where t is the diffusion time, d is the diffusion coefficient, and l is the diffusion length), reaction time was in fact determined by diffusion length. In our tubular DNM sensing system, reaction time was calculated as 1000 s, which well agreed with the simulation prediction of 900 s. We also explored the effect of flow velocity on DNA hybridization. The motion of target-analyte solution was a pressure-driven flow under various velocities. As shown in Figure 3C, the reaction time t of the target analyte varied with velocity υ through a microchannel over a tubular sensing interface. The target analytes were thus forced to diffuse into the depleted zone to maintain their concentration profile at the sensing interface until the sensing probes were completely consumed. Thus, reaction time was determined by the diffusion velocity of target analytes.[23] The complete reaction time for all sensing probes at the tubular interface was simulated as 900, 160, 30, and 10 s, corresponding to velocities of 0.01, 0.1, 1, and 10 mm/s, respectively. Simulation results were consistent with the decreasing trend of the

experimental reaction time from 30 min to 5 min and largely surpassed the experimental values under corresponding flow velocities.

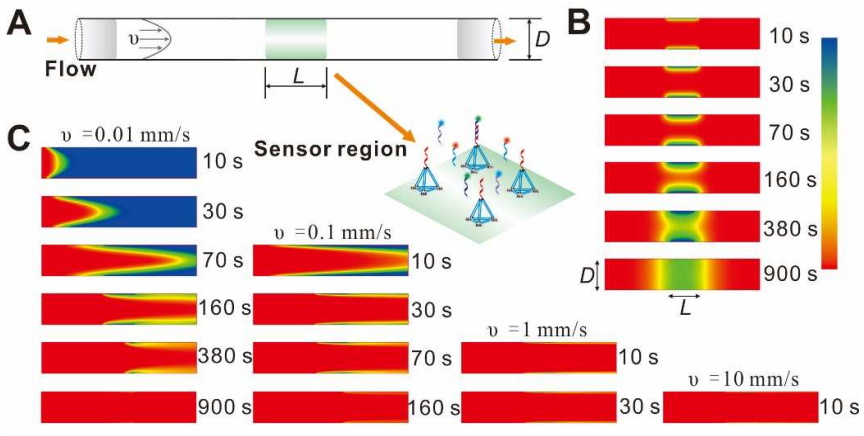

Figure 3. Theoretical studies on the bubble-mediated shuttle reaction inside microchannels. (A) Schematic of analyte solution flowing through the tubular sensing surface. (B) Effect of purely diffusive flux with a setup velocity υ of 0 mm/s under a series of reaction times, including 10, 30, 70, 160, 380, and 900 s. (C) Effect of flow velocity on DNA hybridization.

To realize multiplex detection with a single device, we then designed a tubular DNM sensor by sequentially immobilizing three types of TSPs (TSP-Hg^{2+}, TSP-Ag^{+} and TSP-Pb^{2+}) inside microchannels, as schematically illustrated in Figure 4A. We further used this DNM sensor for the multiplex assay of heavy-metal ions in samples mimicking real-world applications (metal ions spiked in river water). The intense fluorescence signals enabled a direct readout from the microscopic fluorescent images. We then compared the microscopic fluorescent images of the microchannel recorded for a series of samples (Figure 4B). The addition of single analyte was defined as "+" state, and the "–" state corresponds to an absence of analytes. Therefore, the output was "– – –" when neither

analyte was introduced, corresponding to a blank control (row 1, column 1). The addition of 50 nM Hg^{2+}, 50 nM Ag^{+}, or 500 nM Pb^{2+} caused fluorescence variations in corresponding DNM sensing spots, which can be defined as single analyte references (rows 2–4 and column 1). Based on the above results, this DNM sensor can thus be used to realize multiplex detection. For instance, when both Hg^{2+} and Ag^{+} were simultaneously spiked in river water, the output became "+ + –" (row 1, column 2). Similar results can be obtained when Hg^{2+} and Pb^{2+} ("+ – +", row 2, column 2), or Ag^{2+} and Pb^{2+} ("– + +", row 3, column 2) were spiked in river water sample. Finally, the addition of all three metal ions resulted in intense fluorescence in all DNM sensing spots, leading to a "+ + +" state (row 4, column 2). As shown in Table S1, the recoveries of Hg^{2+}, Ag^{+} and Pb^{2+} in the twelve different solutions for each sample were over the range of 79.74-112.7%. These results confirmed that the DNM sensor could be used to simultaneously (or individually) detect Hg^{2+}, Ag^{+} and Pb^{2+} in river water. In addition, the excellent sensing performance of the DNM sensor is also competitive when compared with most other methods as summarized in Table 3.[7,66-72] Taken together, in view of its remarkable simplicity, our DNM sensor can be readily applicable as a quick in-field screening tool for monitoring environmental pollution.

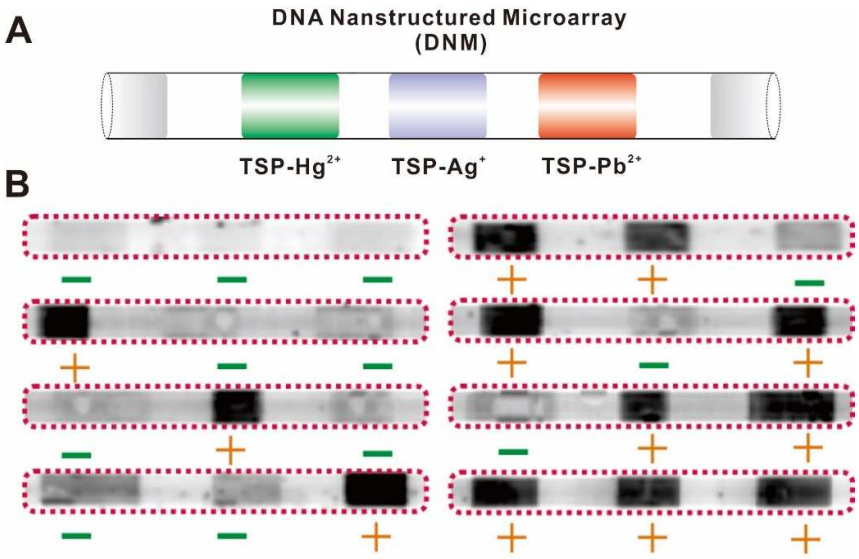

Figure 4. Tubular DNM sensor for the multiplex assay of heavy-metal ions in metal ions spiked river water sample. (A) Schematic of a tubular DNM sensor by immobilizing three types of TSPs inside microchannels for the simultaneous detection of Hg^{2+}, Ag^{+}, and Pb^{2+}. (B) Fluorescent images of DNM sensing spots recorded from various river water samples spiked with different combinations of Hg^{2+}, Ag^{+}, and Pb^{2+}.

Table 3. Analytical Performances of Recent Methods for Simultaneous Detection of Heavy-Metal Ions

Detection methods	Strategy	Detection limit			Sensor mode	Ref
		Ag^{+}	Hg^{2+}	Pb^{2+}		
electrochemistry	DNA Modified Fe3O4@Au Magnetic Nanoparticles	3.4 nM	1.7 nM	/	Turn-on	7
SERS	Oligonucleotide-Functionalized Core/Shell Magnetic Silica Sphere@Au Nanoparticles	1 nM	100 pM	/	Turn-on	66
fluorescence	Nucleic Acid Functionalized CdSe/ZnS Quantum Dots	1 μM	10 nM	/	Turn-off	67
fluorescence	DNA aptamer on quantum dot-based	2.5 nM	1.8 nM	/	Turn-off	68
fluorescence	Nuclease-resistant DNA aptamer on gold nanoparticles	/	121 pM	128 pM	Turn-on	69
fluorescence	DNA aptamer on upconversion nanoparticles	/	150 pM	50 pM	Turn-on	70

fluorescence	the self-assembly of DNA sequences	100 nM	100 nM	20 nM	Turn-on	71
fluorescence	aptamer biosensor based on multi-walled carbon nanotube	18 nM	15 nM	20 nM	Turn-on	72
fluorescence	DNM sensor	10 nM	10 nM	20 nM	Turn-on	this work

CONCLUSION

We demonstrated a simple and efficient analytical platform consisting of spatially resolved 3D tubular DNM functionalized microchannel that can rapidly, sensitively, and selectively detect multiplex heavy-metal ions. This DNM sensor possessed several important advantages. First, we established a DNM sensing interface that allowed for the sensitive and selective detection of multiple metal ions (including Hg^{2+}, Ag^{+}, and Pb^{2+}) in a single microchannel device. Second, the utilization of bubble-mediated shuttle reaction inside microchannel significantly shortened the reaction time to only 5 min. Furthermore, the intense fluorescence intensity enabled a simple optical readout. These attractive features rendered our DNM sensing platform particularly suitable for building POCT. We demonstrated a "proof-of-concept" study on the multiplex detection of heavy-metal ions in contaminated river water samples. Third, our DNM sensor can be inherently generalizable to the detection of virtually any target by the combination of aptamer-based assays. Therefore, given these advantages, we believe that this DNM sensor has enormous potential for rapid field detection in environmental analysis and analytical chemistry.

ASSOCIATED CONTENT

Supporting Information.

Procedures for fabrication of DNM functionalized micro-channel; Recoveries of the ions detection for environmental samples.

This material is available free of charge via the Internet at http://pubs.acs.org.

AUTHOR INFORMATION

Corresponding Author

E-mail: hongc@xmu.edu.cn; peihao@chem.ecnu.edu.cn

Author Contributions

‡The authors have equal contribution to this work.

ACKNOWLEDGMENT

This work was supported by the National Natural Science Foundation of China (21505045, 21675167, 21373260, 21305034, 31571014), the Shanghai Pujiang Program (15PJ1401800, 16PJ1402700), China Postdoctoral Science Foundation (2015M581565), the introduction of major R&D projects of Fujian province (No. 2014I2005), the Natural Science Foundation of Fujian Province of China (2015J01064), Academy of Finland (297580), Jane and Aatos Erkko Foundation (4704010).

REFERENCES

(1) Aragay, G.; Pons, J.; Merkoçi, A. Recent Trends in Macro-, Micro-, and Nanomaterial-Based Tools and Strategies for Heavy-Metal Detection. *Chem. Rev.* **2011**, *111*, 3433-3458.

(2) Chai, X.; Zhou, X.; Zhu, A.; Zhang, L.; Qin, Y.; Shi, G.; Tian, Y. A Two-Channel Ratiometric Electrochemical Biosensor for In Vivo Monitoring of Copper Ions in a Rat Brain Using Gold Truncated Octahedral Microcages. *Angew. Chem. Int. Ed.* **2013**, *52*, 8129-8133.

(3) Zhu, A.; Qu, Q.; Shao, X.; Kong, B.; Tian, Y. Carbon-Dot-Based Dual-Emission Nanohybrid Produces a Ratiometric Fluorescent Sensor for In Vivo Imaging of Cellular Copper Ions. *Angew. Chem. Int. Ed.* **2012**, *124*, 7297-7301.

(4) Vasyukov, D.; Anahory, Y.; Embon, L.; Halbertal, D.; Cuppens, J.; Neeman, L.; Finkler, A.; Segev, Y.; Myasoedov, Y.; Rappaport, M. L.; Huber, M. E.; Zeldov, E. A Scanning Superconducting Quantum Interference Device with Single Electron Spin Sensitivity. *Nat. Nanotechnol.* **2013**, *8*, 639-644.

(5) Tian, Y.; Wang, Y.; Xu, Y.; Liu, Y.; Li, D.; Fan, C. A Highly Sensitive Chemiluminescence Sensor for Detecting Mercury (II) Ions: a Combination of Exonuclease III-aided Signal Amplification and Graphene Oxide-assisted Background Reduction. *Sci. China-Chem.* **2015**, *58*, 514-518.

(6) Tian, T.; Zhang, J.-C.; Lei, H.-Z.; Zhu, Y.; Shi, J.-Y.; Hu, J.; Huang, Q.; Fan, C.-H.; Sun, Y.-H. Synchrotron Radiation X-ray Fluorescence Analysis of Fe, Zn and Cu in Mice Brain Associated with Parkinson's Disease. *Nucl. Sci. Tech.* **2015**, *26*.

(7) Miao, P.; Tang, Y.; Wang, L. DNA Modified Fe_3O_4@Au Magnetic Nanoparticles as Selective Probes for Simultaneous Detection of Heavy Metal Ions. *ACS Appl. Mater. Interfaces* **2017**, *9*, 3940-3947.

(8) Seenivasan, R.; Chang, W.-J.; Gunasekaran, S. Highly Sensitive Detection and

Removal of Lead Ions in Water Using Cysteine-Functionalized Graphene Oxide/Polypyrrole Nanocomposite Film Electrode. *ACS Appl. Mater. Interfaces* **2015**, *7*, 15935-15943.

(9) Chin, C. D.; Laksanasopin, T.; Cheung, Y. K.; Steinmiller, D.; Linder, V.; Parsa, H.; Wang, J.; Moore, H.; Rouse, R.; Umviligihozo, G.; Karita, E.; Mwambarangwe, L.; Braunstein, S. L.; van de Wijgert, J.; Sahabo, R.; Justman, J. E.; El-Sadr, W.; Sia, S. K. Microfluidics-based Diagnostics of Infectious Diseases In the Developing World. *Nat. Med.* **2011**, *17*, 1015-1019.

(10) Das, J.; Cederquist, K. B.; Zaragoza, A. A.; Lee, P. E.; Sargent, E. H.; Kelley, S. O. An Ultrasensitive Universal Detector Based on Neutralizer Displacement. *Nat. Chem.* **2012**, *4*, 642-648.

(11) Yang, F.; Zuo, X.; Li, Z.; Deng, W.; Shi, J.; Zhang, G.; Huang, Q.; Song, S.; Fan, C. A Bubble-Mediated Intelligent Microscale Electrochemical Device for Single-Step Quantitative Bioassays. *Adv. Mater.* **2014**, *26*, 4671-4676.

(12) Men, D.; Zhou, J.; Li, W.; Leng, Y.; Chen, X.; Tao, S.; Zhang, X.-E. Fluorescent Protein Nanowire-Mediated Protein Microarrays for Multiplexed and Highly Sensitive Pathogen Detection. *ACS Appl. Mater. Interfaces* **2016**, *8*, 17472-17477.

(13) Campàs, M.; Katakis, I. DNA Biochip Arraying, Detection and Amplification Strategies. *TrAC Trend Anal. Chem.* **2004**, *23*, 49-62.

(14) Yu, X.; LaBaer, J. High-throughput Ddentification of Proteins With AMPylation Using Self-assembled Human Protein (NAPPA) Microarrays. *Nat. Protoc.* **2015**, *10*, 756-767.

(15) Li, Z.; Zhao, B.; Wang, D.; Wen, Y.; Liu, G.; Dong, H.; Song, S.; Fan, C. DNA

Nanostructure-Based Universal Microarray Platform for High-Efficiency Multiplex Bioanalysis in Biofluids. *ACS Appl. Mater. Interfaces* **2014**, *6*, 17944-17953.

(16) Hong, Y.; Wu, M.; Chen, G.; Dai, Z.; Zhang, Y.; Chen, G.; Dong, X. 3D Printed Microfluidic Device with Microporous Mn_2O_3-Modified Screen Printed Electrode for Real-Time Determination of Heavy Metal Ions. *ACS Appl. Mater. Interfaces* **2016**, *8*, 32940-32947.

(17) Kim, J.; Jang, M.; Lee, K. G.; Lee, K.-S.; Lee, S. J.; Ro, K.-W.; Kang, I. S.; Do Jeong, B.; Park, T. J.; Kim, H.-J.; Lee, J. Plastic-Chip-Based Magnetophoretic Immunoassay for Point-of-Care Diagnosis of Tuberculosis. *ACS Appl. Mater. Interfaces* **2016**, *8*, 23489-23497.

(18) Qu, X.; Lin, R.; Chen, H. Microfluidic Chip Based Microarray Analysis. *Prog. Chem.* **2011**, *23*, 221-230.

(19) Long, H.; Harley-Trochimczyk, A.; Cheng, S.; Hu, H.; Chi, W. S.; Rao, A.; Carraro, C.; Shi, T.; Tang, Z.; Maboudian, R. Nanowire-Assembled Hierarchical $ZnCo_2O_4$ Microstructure Integrated with a Low-Power Microheater for Highly Sensitive Formaldehyde Detection. *ACS Appl. Mater. Interfaces* **2016**, *8*, 31764-31771.

(20) Weiler, M.; Menzel, C.; Pertsch, T.; Alaee, R.; Rockstuhl, C.; Pacholski, C. Bottom-Up Fabrication of Hybrid Plasmonic Sensors: Gold-Capped Hydrogel Microspheres Embedded in Periodic Metal Hole Arrays. *ACS Appl. Mater. Interfaces* **2016**, *8*, 26392-26399.

(21) Lei, Z.; Gao, J.; Liu, X.; Liu, D.; Wang, Z. Poly(glycidyl methacrylate-co-2-hydroxyethyl methacrylate) Brushes as Peptide/Protein Microarray Substrate for Improving Protein Binding and Functionality. *ACS Appl. Mater. Interfaces*

2016, *8*, 10174-10182.

(22) Wang, S.; Deng, S.; Cai, X.; Hou, S.; Li, J.; Gao, Z.; Li, J.; Wang, L.; Fan, C. Superresolution Imaging of Telomeres With Continuous Wave Stimulated Emission Depletion (STED) Microscope. *Sci. China-Chem.* **2016**, *59*, 1519-1524.

(23) Squires, T. M.; Messinger, R. J.; Manalis, S. R. Making It Stick: Convection, Reaction and Diffusion in Surface-based Biosensors. *Nat. Biotechnol.* **2008**, *26*, 417-426.

(24) Sheehan, P. E.; Whitman, L. J. Detection Limits for Nanoscale Biosensors. *Nano Lett.* **2005**, *5*, 803-807.

(25) Su, S.; Fan, J.; Xue, B.; Yuwen, L.; Liu, X.; Pan, D.; Fan, C.; Wang, L. DNA-Conjugated Quantum Dot Nanoprobe for High-Sensitivity Fluorescent Detection of DNA and Micro-RNA. *ACS Appl. Mater. Interfaces* **2014**, *6*, 1152-1157.

(26) Pei, H.; Li, F.; Wan, Y.; Wei, M.; Liu, H.; Su, Y.; Chen, N.; Huang, Q.; Fan, C. Designed Diblock Oligonucleotide for the Synthesis of Spatially Isolated and Highly Hybridizable Functionalization of DNA-gold Nanoparticle Nanoconjugates. *J. Am. Chem. Soc.* **2012**, *134*, 11876-11879.

(27) Zhu, D.; Pei, H.; Chao, J.; Su, S.; Aldalbahi, A.; Rahaman, M.; Wang, L.; Wang, L.; Huang, W.; Fan, C.; Zuo, X. Poly-adenine-based Programmable Engineering of Gold Nanoparticles for Highly Regulated Spherical DNAzymes. *Nanoscale* **2015**, *7*, 18671-18676.

(28) Pei, H.; Li, J.; Lv, M.; Wang, J.; Gao, J.; Lu, J.; Li, Y.; Huang, Q.; Hu, J.; Fan, C. A Graphene-based Sensor Array for High-precision and Adaptive Target Identification With Ensemble Aptamers. *J. Am. Chem. Soc.* **2012**, *134*, 13843-13849.

(29)Kumar, V.; Brent, J. R.; Shorie, M.; Kaur, H.; Chadha, G.; Thomas, A. G.; Lewis, E. A.; Rooney, A. P.; Lan, N.; Zhong, X. L.; Burke, M. G.; Haigh, S. J.; Walton, A.; McNaughter, P. D.; Tedstone, A. A.; Savjani, N.; Muryn, C. A.; O'Brien, P.; Ganguli, A. K.; Lewis, D. J.; Sabherwal, P. Nanostructured Aptamer-Functionalized Black Phosphorus Sensing Platform for Label-Free Detection of Myoglobin, a Cardiovascular Disease Biomarker. *ACS Appl. Mater. Interfaces* **2016**, *8*, 22860-22868.

(30)Lin, M.; Wang, J.; Zhou, G.; Wang, J.; Wu, N.; Lu, J.; Gao, J.; Chen, X.; Shi, J.; Zuo, X.; Fan, C. Programmable Engineering of a Biosensing Interface with Tetrahedral DNA Nanostructures for Ultrasensitive DNA Detection. *Angew. Chem. Int. Ed.* **2015**, *54*, 2151-2155.

(31)Dong, S.; Zhao, R.; Zhu, J.; Lu, X.; Li, Y.; Qiu, S.; Jia, L.; Jiao, X.; Song, S.; Fan, C.; Hao, R.; Song, H. Electrochemical DNA Biosensor Based on a Tetrahedral Nanostructure Probe for the Detection of Avian Influenza A (H7N9) Virus. *ACS Appl. Mater. Interfaces* **2015**, *7*, 8834-8842.

(32)Kim, J.; Vu, B.; Kourentzi, K.; Willson, R. C.; Conrad, J. C. Increasing Binding Efficiency via Reporter Shape and Flux in a Viral Nanoparticle Lateral-Flow Assay. *ACS Appl. Mater. Interfaces* **2017**, *9*, 6878-6884.

(33)Zhang, L.; Fang, M. Nanomaterials in Pollution Trace Detection and Environmental Improvement. *Nano Today* **2010**, *5*, 128-142.

(34)Farimani, A. B.; Dibaeinia, P.; Aluru, N. R. DNA Origami-Graphene Hybrid Nanopore for DNA Detection. *ACS Appl. Mater. Interfaces* **2017**, *9*, 92-100.

(35)Kelley, S. O.; Mirkin, C. A.; Walt, D. R.; Ismagilov, R. F.; Toner, M.; Sargent, E. H.

Advancing the Speed, Sensitivity and Accuracy of Biomolecular Detection Using Multi-length-scale Engineering. *Nat. Nanotechnol.* **2014**, *9*, 969-980.

(36) Kim, J.; You, J. B.; Nam, S. M.; Seo, S.; Im, S. G.; Lee, W. Rollable Microfluidic Systems with Micrometer-Scale Bending Radius and Tuning of Device Function with Reconfigurable 3D Channel Geometry. *ACS Appl. Mater. Interfaces* **2017**, DOI: 10.1021/acsami.7b00741.

(37) Li, S.; Liu, Y.-Y.; Liu, L.-J.; Hu, Q.-X. A Versatile Method for Fabricating Tissue Engineering Scaffolds with a Three-Dimensional Channel for Prevasculature Networks. *ACS Appl. Mater. Interfaces* **2016**, *8*, 25096-25103.

(38) Wang, G.; Li, K.; Purcell, F. J.; Zhao, D.; Zhang, W.; He, Z.; Tan, S.; Tang, Z.; Wang, H.; Reichnianis, E. Three-Dimensional Clustered Nanostructures for Microfluidic Surface-Enhanced Raman Detection. *ACS Appl. Mater. Interfaces* **2016**, *8*, 24974-24981.

(39) Pei, H.; Zuo, X.; Zhu, D.; Huang, Q.; Fan, C. Functional DNA Nanostructures for Theranostic Applications. *Acc. Chem. Res.* **2014**, *47*, 550-559.

(40) Pei, H.; Zuo, X.; Pan, D.; Shi, J.; Huang, Q.; Fan, C. Scaffolded Biosensors with Designed DNA Nanostructures. *NPG Asia Mater.* **2013**, *5*, e51.

(41) Yao, G.; Li, J.; Chao, J.; Pei, H.; Liu, H.; Zhao, Y.; Shi, J.; Huang, Q.; Wang, L.; Huang, W.; Fan, C. Gold-Nanoparticle-Mediated Jigsaw-Puzzle-like Assembly of Supersized Plasmonic DNA Origami. *Angew. Chem. Int. Ed.* **2015**, *54*, 2966-2969.

(42) Chao, J.; Zhang, Y.; Zhu, D.; Liu, B.; Cui, C.; Su, S.; Fan, C.; Wang, L. Hetero-assembly of Gold Nanoparticles on a DNA Origami Template. *Sci. China-Chem.* **2016**, *59*, 730-734.

(43)Jiang, D.; Sun, Y.; Li, J.; Li, Q.; Lv, M.; Zhu, B.; Tian, T.; Cheng, D.; Xia, J.; Zhang, L.; Wang, L.; Huang, Q.; Shi, J.; Fan, C. Multiple-Armed Tetrahedral DNA Nanostructures for Tumor-Targeting, Dual-Modality in Vivo Imaging. *ACS Appl. Mater. Interfaces* **2016**, *8*, 4378-4384.

(44) Du, W.-B.; Fang, Q.; Fang, Z.-L. Microfluidic Sequential Injection Analysis in a Short Capillary. *Anal. Chem.* **2006**, *78*, 6404-6410.

(45) Du, W.-B.; Fang, Q.; He, Q.-H.; Fang, Z.-L. High-Throughput Nanoliter Sample Introduction Microfluidic Chip-Based Flow Injection Analysis System with Gravity-Driven Flows. *Anal. Chem.* **2005**, *77*, 1330-1337.

(46) Ge, Z.; Pei, H.; Wang, L.; Song, S.; Fan, C. Electrochemical Single Nucleotide Polymorphisms Genotyping On Surface Immobilized Three-dimensional Branched DNA Nanostructure. *Sci. China-Chem.* **2011**, *54*, 1273-1276.

(47) Pei, H.; Wan, Y.; Li, J.; Hu, H.; Su, Y.; Huang, Q.; Fan, C. Regenerable Electrochemical Immunological Sensing at DNA Nanostructure-decorated Gold Surfaces. *Chem. Commun.* **2011**, *47*, 6254-6256.

(48) Qu, X.; Wang, Y.; Shi, Z.; Fu, G.; Zeng, X.; Li, X.; Chen, H. Probe Droplet Arrays Generated in the Capillary for Microarray Analysis. *Biosens. Bioelectron.* **2012**, *38*, 342-347.

(49) Gupta, R.; Reifenberger, R. G.; Kulkarni, G. U. Cellphone Camera Imaging of a Periodically Patterned Chip as a Potential Method for Point-of-Care Diagnostics. *ACS Appl. Mater. Interfaces* **2014**, *6*, 3923-3929.

(50) Zhang, Y.; Liu, W.; Zhang, W.; Yu, S.; Yue, X.; Zhu, W.; Zhang, D.; Wang, Y.; Wang, J.

DNA-mediated gold nanoparticle signal transducers for combinatorial logic operations and heavy metal ions sensing. *Biosens. Bioelectron.* **2015**, *72*, 218-224.

(51) Willner, I.; Zayats, M. Electronic Aptamer-Based Sensors. *Angew. Chem. Int. Ed.* **2007**, *46*, 6408-6418.

(52) Pei, H.; Lu, N.; Wen, Y.; Song, S.; Liu, Y.; Yan, H.; Fan, C. A DNA Nanostructure-based Biomolecular Probe Carrier Platform for Electrochemical Biosensing. *Adv. Mater.* **2010**, *22*, 4754-4758.

(53) Pei, H.; Liang, L.; Yao, G.; Li, J.; Huang, Q.; Fan, C. Reconfigurable Three-Dimensional DNA Nanostructures for the Construction of Intracellular Logic Sensors. *Angew. Chem. Int. Ed.* **2012**, *124*, 9154-9158.

(54) Lu, N.; Pei, H.; Ge, Z.; Simmons, C. R.; Yan, H.; Fan, C. Charge Transport Within a Three-dimensional DNA Nanostructure Framework. *J. Am. Chem. Soc.* **2012**, *134*, 13148-13151.

(55) Li, J.; Pei, H.; Zhu, B.; Liang, L.; Wei, M.; He, Y.; Chen, N.; Li, D.; Huang, Q.; Fan, C. Self-assembled Multivalent DNA Nanostructures for Noninvasive Intracellular Delivery of Immunostimulatory CpG Oligonucleotides. *ACS Nano* **2011**, *5*, 8783-8789.

(56) Xue, X.; Wang, F.; Liu, X. One-Step, Room Temperature, Colorimetric Detection of Mercury (Hg^{2+}) Using DNA/Nanoparticle Conjugates. *J. Am. Chem. Soc.* **2008**, *130*, 3244-3245.

(57) Liu, J.; Lu, Y. Rational Design of "Turn-On" Allosteric DNAzyme Catalytic Beacons for Aqueous Mercury Ions with Ultrahigh Sensitivity and Selectivity. *Angew. Chem. Int. Ed.* **2007**, *119*, 7731-7734.

(58)Clever, G. H.; Kaul, C.; Carell, T. DNA–Metal Base Pairs. *Angew. Chem. Int. Ed.* **2007**, *46*, 6226-6236.

(59) Pandeeswar, M.; Senanayak, Satyaprasad P.; Govindaraju, T. Nanoarchitectonics of small molecule and DNA for ultrasensitive detection of mercury. *ACS Appl. Mater. Interfaces* **2016**, *8*, 30362-30371.

(60) Katz, S. The reversible reaction of Hg (Ii) and double stranded polynucleotides a step-function theory and its significance. *Biochim. Biophys. Acta, Spec. Sect. Nucleic Acids Relat. Subj.* **1963**, *68*, 240-253.

(61) Park, K. S.; Lee, C. Y.; Park, H. G. Metal ion triggers for reversible switching of DNA polymerase, *Chem. Commun.* **2016**, *52*, 4868-4871.

(62) Wei, C.-W.; Cheng, J.-Y.; Huang, C.-T.; Yen, M.-H.; Young, T.-H. Using a Microfluidic Device for 1 μl DNA Microarray Hybridization in 500 s. *Nucleic Acids Res.* **2005**, *33*, e78.

(63) Chen, H.; Wang, L.; Li, P. C. H. Nucleic Acid Microarrays Created in the Double-spiral Format on a Circular Microfluidic Disk. *Lab Chip* **2008**, *8*, 826-829.

(64) Xu, H.; Xu, P.; Gao, S.; Zhang, S.; Zhao, X.; Fan, C.; Zuo, X. Highly Sensitive Recognition of Pb^{2+} Using Pb^{2+} Triggered Exonuclease Aided DNA Recycling. *Biosens. Bioelectron.* **2013**, *47*, 520-523.

(65) Wang, F.; Wu, Y.; Zhan, S.; He, L.; Zhi, W.; Zhou, X.; Zhou, P. A Simple and Sensitive Colorimetric Detection of Silver Ions Based on Cationic Polymer-Directed AuNPs Aggregation. *Aust. J. Chem.* **2013**, *66*, 113-118.

(66) Liu, M.; Wang, Z.; Zong, S.; Chen, H.; Zhu, D.; Wu, L.; Hu, G.; Cui, Y. SERS detection and removal of mercury(II)/silver(I) using oligonucleotide-functionalized

core/shell magnetic silica sphere@Au nanoparticles. *ACS Appl. Mater. Interfaces* **2014**, *6*, 7371-7379.

(67) Freeman, R.; Finder, T.; Willner, I. Multiplexed analysis of Hg^{2+} and Ag^{+} ions by nucleic acid functionalized CdSe/ZnS quantum dots and their use for logic gate operations. *Angew. Chem. Int. Ed.* **2009**, *48*, 7818–7821.

(68) Hao, C.; Xua, L.; Xing, C.; Kuang, H.; Wang, L.; Xu, C. Oligonucleotide-based fluorogenic sensor for simultaneous detection of heavy metal ions. *Biosens. Bioelectron.* **2012**, *36*, 174-178.

(69) Chung, C. H.; Kima, J. H.; Jung, J.; Chung, B. H. Nuclease-resistant DNA aptamer on gold nanoparticles for the simultaneous detection of Pb^{2+} and Hg^{2+} in human serum. *Biosens. Bioelectron.* **2013**, *41*, 827-832.

(70) Wu, S.; Duan, N.; Shi, Z.; Fang, C.; Wang, Z. Dual fluorescence resonance energy transfer assay between tunable upconversion nanoparticles and controlled gold nanoparticles for the simultaneous detection of Pb^{2+} and Hg^{2+}. *Talanta* **2014**, *128*, 327-336.

(71) Xia, J.; Lin, M.; Zuo, X.; Su, S.; Wang, L.; Huang, W.; Fan, C.; Huang, Q. Metal ion-mediated assembly of DNA nanostructures for cascade fluorescence resonance energy transfer-based fingerprint analysis. *Anal. Chem.* **2014**, *86*, 7084-7087.

(72) Wang, S.; Si, S. Aptamer biosensing platform based on carbon nanotube long-range energy transfer for sensitive, selective and multicolor fluorescent heavy metal ion analysis. *Anal. Methods* **2013**, *5*, 2947-2953.

TOC

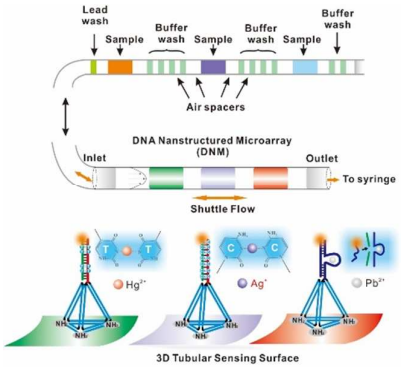
Lead wash
Sample
Buffer wash
Sample
Buffer wash
Sample
Buffer wash
Air spacers
DNA Nanstructured Microarray (DNM)
Inlet
Outlet
To syringe
Shuttle Flow
Hg2+
Ag+
Pb2+
3D Tubular Sensing Surface